EVENT SHAPE ENGINEERING AND STUDY OF HIGH-MULTIPLICITY PROTON+PROTON COLLISIONS AT $\sqrt{s}$ = 13 TeV USING PYTHIA 8.2

M.Sc. THESIS

By

Ashish Bisht

DISCIPLINE OF PHYSICS

INDIAN INSTITUTE OF TECHNOLOGY INDORE

June 2019

EVENT SHAPE ENGINEERING AND STUDY OF HIGH-MULTIPLICITY PROTON+PROTON COLLISIONS AT $\sqrt{s}$ = 13 TeV USING PYTHIA 8.2

A THESIS

Submitted in partial fulfillment of the

requirements for the award of the degree

of

Master of Science

by

Ashish Bisht

under the guidance of

Dr. Raghunath Sahoo

DISCIPLINE OF PHYSICS

INDIAN INSTITUTE OF TECHNOLOGY INDORE

June 2019

INDIAN INSTITUTE OF TECHNOLOGY INDORE

CANDIDATE'S DECLARATION

Indian Institute of Technology Indore
Thesis submitted on 28/06/19
Administrative Officer

I hereby certify that the work which is being presented in the thesis entitled **"Event shape engineering and study of high-multiplicity proton+proton collisions at $\sqrt{s}$ = 13 TeV using PYTHIA 8.2"** in the partial fulfilment of the requirements for the award of the degree of MASTER OF SCIENCE and submitted in the **DISCIPLINE OF PHYSICS, Indian Institute of Technology Indore**, is an authentic record of my own work carried out during the time period from JULY 2018 to JUNE 2019 under the supervision of Dr. Raghunath Sahoo, Associate Professor, Indian Institute of Technology Indore. The matter presented in this thesis has not been submitted by me for the award of any other degree of this or any other institute. In case of any plagiarism, as the sole author, I shall stay responsible.

(ASHISH BISHT)

This is to certify that the above statement made by the candidate is correct to the best of my knowledge.

M.Sc. Thesis Supervisor

(Dr. Raghunath Sahoo)

Ashish Bisht has successfully given his M.Sc. Oral Examination held on 21. June - 2019

(M.Sc. Thesis Supervisor)

Date: 26.06.19

(PSPC Member 1.) Subhendu Rakshit

Date: 26/06/2019

(Convener, DPGC)

Date: 26/6/19

(PSPC Member 2.) K. Eswaran M

Date: 26/06/19

ACKNOWLEDGEMENT

First and the foremost I would like to express my deepest gratitude to my supervisor Prof. Raghunath Sahoo not only for his support and guidance, but also for giving me the opportunity to undertake this exciting project. His guidance and enthusiasm kept me motivated during my work. He came forward in each moment whenever I was in problem and suggested the right way to move forward. I am thankful to him for sharing his valuable time. Without him this project was not possible.

I would like to thank my PSPC committee members Prof. Subhendu Rakshit and Prof. Eswara Prasad Korimilli for their support and motivation. I am very grateful to the Physics Department of IIT Indore for providing me all the required facilities.

I am very thankful to all the members of the Experimental High-Energy Physics group at IIT Indore. I would like to express my thanks to Dr. Arvind Khuntia and Sushanta Tripathy with whom I shared my project work. I would especially like to thank Dr. Arvind Khuntia for his help in technical problems in PYTHIA, ROOT and for all the discussions and fun on weekends. I would also like to thank everyone around me for their moral support and blessings.

The support I got from my parents, my brother and my friend Kapil is something beyond acknowledgement. They were always with me, and encouraged me in every possible way.

ASHISH BISHT

Dedicated to my parents

and

my brother

ABSTRACT

Earlier pp-collision was considered as the baseline in measurements for heavy-ion collisions. But in the small systems collectivity was observed at LHC energies added to the strangeness enhancement, ridge structure, hardening of p_T-spectra in high-multiplicity events. This suggests a possibility of medium formation in small systems like pp-collision. Color reconnection and Multi-Partonic Interactions can produce medium-like effects and are responsible for collectivity in small systems. It is interesting to look into the QGP-like features, usually found in heavy ion collisions in high-multiplicity proton+proton collisions. Event shape observables are the tools that can be used to study the geometric shapes of energy distribution in any collision experiment. The motivation of this project is to further investigate whether the collective behaviour observed in high energy pp-collisions can be imputed to the formation of Quark-Gluon Plasma (QGP). This is done by using transverse spherocity for the double differential study of several observables with reference to charged-particle multiplicity in high-multiplicity pp-collisions at $\sqrt{s}$= 13 TeV. The different multiplicity pp-events were divided into different transverse spherocity bins in order to probe whether the particle production is dominated by events that are geometrically jet-like or isotropic. This analysis is carried out using PYTHIA 8.2.

The final state charged-particles have been chosen in the acceptance of V0 detector in ALICE at the LHC with pseudorapidity coverage of V0A ($2.8 < \eta < 5.1$) and V0C ($-3.7 < \eta < -1.7$) and these events are divided into ten multiplicity (V0M) classes. To disentangle the jetty (hard) and isotropic (soft) events from the average-shaped events we have applied the spherocity cuts on generated events. The spherocity distribution is selected in the pseudo-rapidity range of $|\eta|< 0.8$. The transverse momentum (p_{T}) spectra for identified particles like pion, kaon, proton and lambda are found in mid-rapidity, $|\eta|< 0.5$ as a function of spherocity and multiplicity. The ratio of jetty and isotropic to spherocity integrated p_{T}-spectra was found to be multiplicity dependent and the crossing point shifts towards higher values of p_{T} as we move from low- to high-multiplicity. We observe a strong dependence on spherocity and multiplicity

for all particles. Further we are interested in the thermodynamics of the system and to obtain the kinetic freeze-out temperature we use thermodynamically consistent Tsallis distribution function and Boltzmann-Gibbs Blast wave function for hadrons in pp-collisions. We analyse the transverse momentum (p_{T}) spectra using these models and study the multiplicity dependence of temperature (T$_{kin}$), q (non-extensive parameter) from Tsallis and T$_{kin}$, β (radial flow) from BGBW model. We observe dependence of extracted parameters on spherocity and charged-particle multiplicity for all particles. With increasing multiplicity, we found that kinetic freeze-out temperature also increases. For heavier particles, this increase was more steeper than lighter particles. In addition to this, we also study the dependence of these parameters on particle mass to observe any mass ordering. It was interesting to see that T$_{kin}$ and β were found to be dependent on mass for highest multiplicity, which is an indication of differential freeze-out scenario.

The thesis is organized as follows: after a brief introduction and motivation to study pp-collisions at the LHC energies in view of QGP-like behaviour in high-multiplicity pp-collisions, small discussion on the QCD, QGP, basic kinematics are discussed in chapter 1. In chapter 2, we discuss about the event shape observable like spherocity and its correlation with multiplicity. Multi-partonic interaction and their role in pp-collisions is also discussed in this chapter with its correlation to multiplicity. In chapter 3 we present the analysis methodology, PYTHIA event generator and its underlying physics, application of Tsallis non-extensive statistics and BGBW in pp-collisions. At the end, chapter 5 summarises our results with important findings.

LIST OF PUBLICATIONS

1. Event Shape Engineering and Multiplicity dependent study of identified particle production in proton+proton collisions at $\sqrt{s} = 13$ TeV using PYTHIA, *Arvind Khuntia, Sushanta Tripathy, **Ashish Bisht**, Raghunath Sahoo*. arXiv:1811.04213, Eur. Phys. J. C (under review)

2. Event shape and Multiplicity dependence of Freeze-out Scenario and System Thermodynamics in Proton+Proton Collisions at $\sqrt{s}$ = 13 TeV, *Sushanta Tripathy, **Ashish Bisht**, Raghunath Sahoo, Arvind Khuntia, Malvika P.S.*. arXiv:1905.07418, Eur. Phys. J. C (under review)

Contents

List of Figures

List of Tables

Chapter 1

Introduction

Atoms are made up of hadrons and leptons, but what hadrons are made up of? Quarks and gluons are bound together by strong forces to make hadrons. A single quark is impossible to be observed in isolation due to the peculiar property of Quantum Chromodynamics (QCD) i.e., confinement. At sufficiently high temperatures the hadronic boundary is dissolved and all the quarks and gluons form a hot dense soup known as Quark Gluon Plasma. It is an exotic phase of matter which is found only at high temperatures and/or energy densities, where quarks and gluons are said to be asympotically free inside it. In ultra-relativistic heavy-ion collisions, we can create QGP and study this exotic matter with deconfined quarks and gluons. Measurements of particle production in proton-proton (p+p) collisions are very important to provide a baseline for understanding the interactions in the QGP created in heavy-ion collisions [1]. Earlier it was believed that proton+proton collisions serve as the baseline measurements for nucleus-nucleus collisions, where scientists try to study the primordial matter, which is composed of quarks and gluons. But the recent findings of strangeness enhancement [2] and ridge structure in high-multiplicity pp-collisions gives a twist in the study of pp-collision. A new direction of physics has emerged from the multiplicity dependent studies of various observables like collective flow, particle ratio etc and we can expect QGP-like system is formed in pp-collisions while studying high-multiplicity events.

The main purpose of this analysis is to see whether pp-collisions can create droplets of QGP and to study the underlying dynamics of particle production, which can put light on the observable effects of high-multiplicity events in proton+proton collisions. This analysis is performed by studying pp-collisions with a center of mass energy $\sqrt{s}$= 13 TeV, generated from PYTHIA 8.2.

1.1 The Standard Model

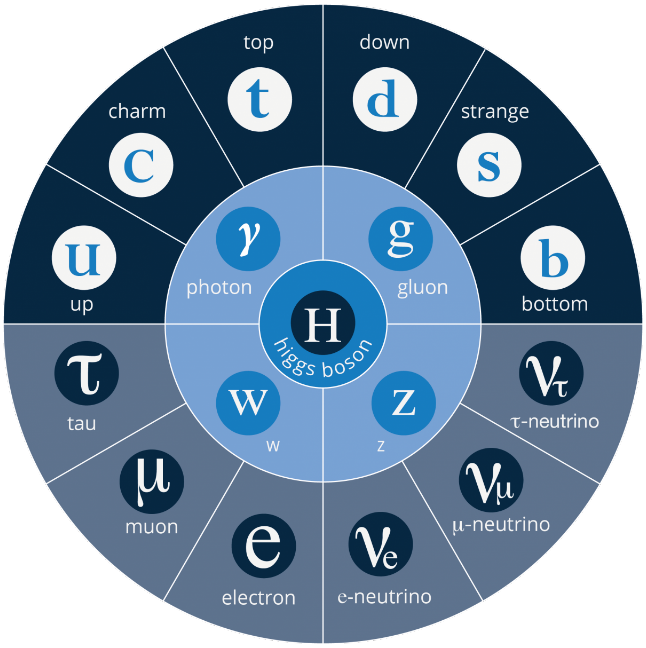

Figure 1.1: Overview of elementary particles in the Standard Model [3]

The Standard Model is a local gauge theory, used to describe all the phenomena of particle physics by unifying the fundamental forces except gravitational force. All the elementary particles and fundamental forces are incorporated in SM. The four fundamental forces in order of increasing strength are as follows:

- Gravitational Force (Dominant in higher mass objects like Black Holes but negligible at subatomic levels)
- Weak Interaction
- Electromagnetic Interaction
- Strong Interaction (dominant in quark level and can be explained using QCD)

Figure 1.1 gives a representation of standard model where the particles are divided into two categories, *fermions* and *bosons*. The outer most circle consists of all fermions and the inner circles consists of all bosons.

1.2 Quantum Chromodynamics

Quantum Chromodynamics is the theory used to explain the interactions between quarks and gluons in a similar way QED explains the interaction between charged particles. The strength of coupling constant α_s has an interesting dependence on the energy of the system. In QED, strength of coupling constant α_{EM} decreases with the distance between the charged particles, but in QCD it is quite opposite. Strength of α_s increases with the distance or decreases with energy (E $\propto$ 1/r). At higher energies the quarks behave as free particles, this is called *asymptotic freedom*. According to this, when the two quarks are separated more, then at some moment the energy will become sufficient to produce another pair of $q\overline{q}$, this process is called pair creation.

1.3 Proton+Proton Collisions

The particle collisions analysed throughout this report are proton+proton (pp) collisions. To understand the underlying mechanism behind pp-collision is crucial as it is the lightest baryon. A proton+proton collision can be seen as simply two singular protons colliding but at higher energies one can view the event as a direct collision between partons residing inside the hadronic boundaries. In pp-collisions two different kinds of processes occur: hard scattering and soft scattering. The soft scattering is associated with collisions where the momentum transfer is very small. Due to the color confinement the partons from each proton are bounded together and the momentum transfer is not sufficient to knock them out free. These types of collisions are mostly elastic in nature. Soft processes are responsible for phenomena such as bulk particle production and hydrodynamic flow. Hard scattering are associated with a large momentum transfer during collisions. These collisions are highly inelastic in nature and the colliding particles as well as produced particles will scatter at large angles in the transverse plane.

1.4 Quark Gluon Plasma

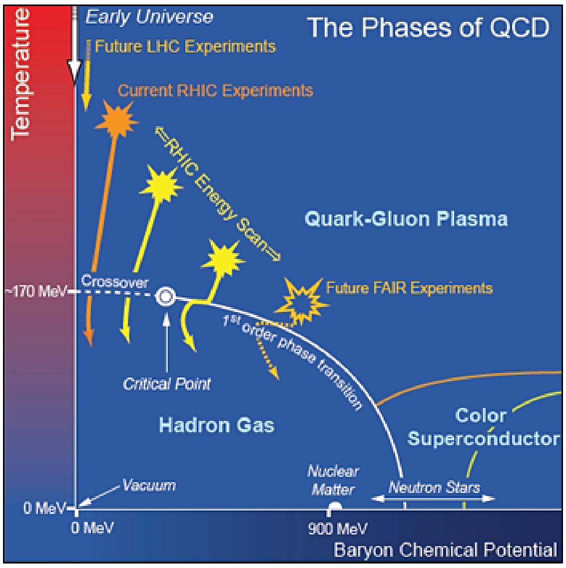

Figure 1.2: Phase Diagram of QCD matter

Quarks and Gluons cannot exist freely due to the color confinement. However, a state of matter was hypothesized where quarks and gluons can be deconfined and can exist freely from their individual hadrons. This new state of matter is known as Quark Gluon Plasma (QGP). During the creation of universe, it is proposed that the matter in the Universe existed as a QGP for a few microseconds after the big bang. The idea is that, by increasing the pressure (merging the hadrons together) and heat (exciting the quarks out of the hadrons), the partons will merge together into one large 'soup' consisting of quarks and gluons. It is believed that the collisions at the LHC may provide enough heat and pressure to produce QGP in the initial state. This state of matter would thus be incredibly hot and dense. However, because of short lifetime of QGP, the associated signatures are indirect in nature.

1.5 Basic Kinematics

To understand the fundamental nature of particles and the interaction between them we have to deal with so many terms and observables that are necessary. In the following section, we shall discuss about these observables [4].

1.5.1 Transverse Momentum, p_T

At colliders the particle detectors are often built concentrically around the accelerator beam-axis where the beam particles travel. The beam direction is chosen to be along z-axis. Transverse observables are Lorentz invariants. The transverse momentum is defined as:

$$p_\mathrm{T} = \sqrt{p_x^2 + p_y^2} \tag{1.1}$$

Before the collision all particles have zero p_T. Thus study of transverse momentum spectra gives a better insight into the physics of particle production. p_T-spectra also gives the information about the system temperature: inverse slope of the spectra being effective temperature of the system.

1.5.2 Rapidity (y) and Pseudorapidity (η)

In the domain of relativistic energies the velocity is non-linear i.e., in successive Lorentz boosts velocities are not simply additive in nature. Rapidity offers the ease of being shape invariant under Lorentz transforms and is additive in nature. Rapidity is defined as:

$$y = \frac{1}{2} ln(\frac{E + p_z c}{E - p_z c}) \tag{1.2}$$

where $\beta = \dfrac{v}{c}$ $\qquad E = \sqrt{p_x^2 c^2 + p_y^2 c^2 + p_z^2 c^2 - m^2 c^4}$

It shows linear behaviour, so a single Lorentz transformation with rapidity y can be decomposed into the n-successive Lorentz transformations with the rapidity $\triangle y$

$$\triangle\, y = \frac{y}{n} \tag{1.3}$$

To measure rapidity, one needs to have the knowledge of both momentum and energy of a particle. This also involves knowing the particle mass and hence the particle identification. This is experimentally highly challenging and for different particle species, the technology of particle detection is different. One thus introduces pseudorapidity to circumvent this problem.

The rapidity for a particle emitted at an angle θ can be written as

$$y = \frac{1}{2} ln \left(\frac{E + p_z}{E - p_z} \right) = \frac{1}{2} ln \left[\frac{\sqrt{m^2 + p^2} + p\, cos\theta}{\sqrt{m^2 + p^2} - p\, cos\theta} \right] \tag{1.4}$$

At very high energy, $p >> m$ and hence

$$y = \frac{1}{2} ln \left[\frac{p + p\, cos\theta}{p - p\, cos\theta} \right] \tag{1.5}$$

$$y \simeq -ln\, tan(\frac{\theta}{2}) \tag{1.6}$$

We define pseudorapidity as

$$\eta \simeq -ln\, tan(\frac{\theta}{2}) \tag{1.7}$$

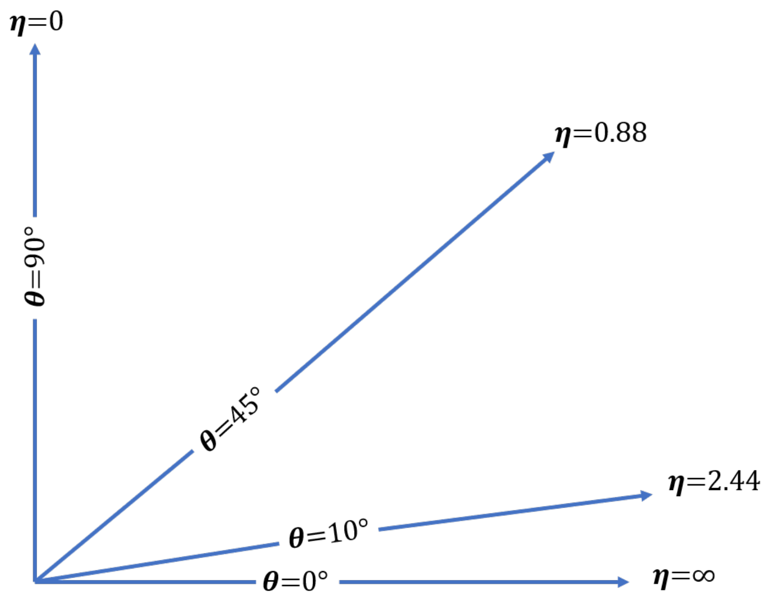

Figure 1.3: Pseudorapidity of particles and their corresponding polar angles

For highly relativistic particles $y \simeq \eta$, pseudorapidity comes handy in collider experiments as η is easier to calculate than y, because it only needs the information of the emission angle.

A relationship between η and y is

$$\frac{dN}{d\eta} = \sqrt{1 - \frac{m^2}{m_T^2 cosh^2 y}} \frac{dN}{dy} \tag{1.8}$$

For massless particles like photons, both η and y curve are the same. m_T is particle's transverse mass which is $m_T = \sqrt{m^2 + p_T^2}$.

1.5.3 Azimuthal and Polar Angles

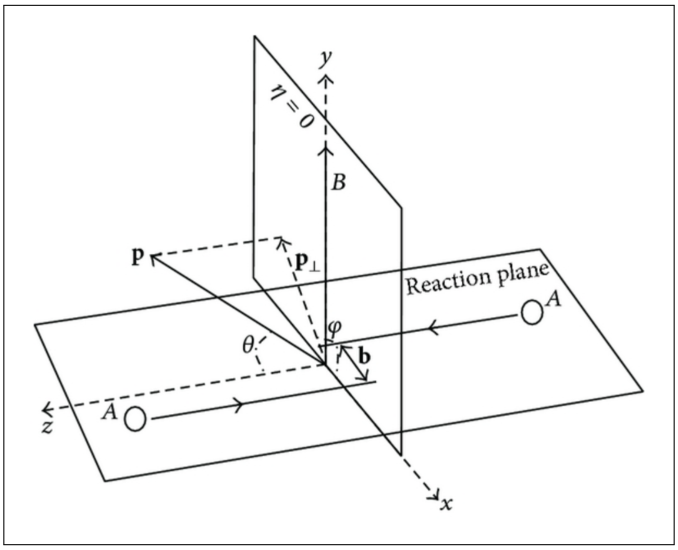

Figure 1.4: Representation of η, ϕ, p_{T} and impact parameter (b) in Reaction-plane

In $\eta - \phi$ coordinate system, the azimuthal angle ϕ is defined as

$$\phi = tan^{-1}\frac{p_y}{p_x} \tag{1.9}$$

The polar angle describes the angle of inclination of particle track from the beam direction (z-axis) and is defined as:

$$\theta = cos^{-1}\frac{p_z}{|\overrightarrow{p}|} = tan^{-1}\frac{|\overrightarrow{p_{\mathrm{T}}}|}{p_z} \tag{1.10}$$

Figure 1.4 gives a clear picture of the detector geometry, beam axis and the chosen $\eta - \phi$ coordinate system.

1.5.4 Multiplicity

Multiplicity refers to the number of tracks or the number of final state particles detected in a collision. Collisions with large number of tracks (high-multiplicity) are indicative of a central head-on collision with higher number of participants. The multiplicity distribution can be used to study the underlying physics of high energy collision experiments.

In fig 1.5 we show the distribution of number of charge particles produced in pp-collisions. We will divide this distribution into ten different multiplicity

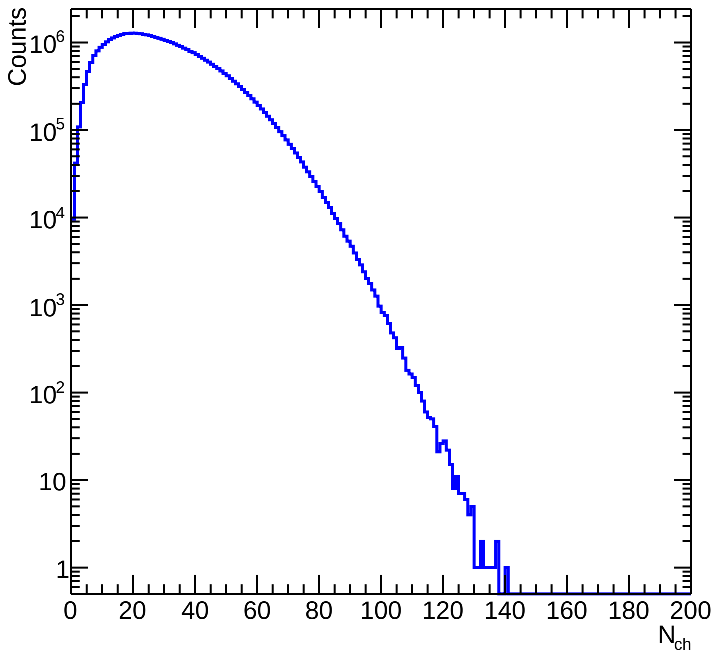

Figure 1.5: Distribution for number of charged particles (N_{ch}) in pp-collisions at $\sqrt{s}$ = 13 TeV using PYTHIA.

bins. Every bin will be the 10% of this distribution. So lowest multiplicity will be containing the events in which less number of charged particles are created while the highest multiplicity will be having events with more number of charged particles. The detailed distribution of multiplicities is given in chapter 3.

Chapter 2

Event Shape engineering and Multi-Partonic Interactions

The geometrical properties of the energy flow in QCD events can be measured using event shapes. Event shapes were among the first observables proposed to test QCD. They play very crucial role in the extraction of the strong coupling from final-state properties. These are essential in tuning the non-perturbative components of Monte Carlo event generators.

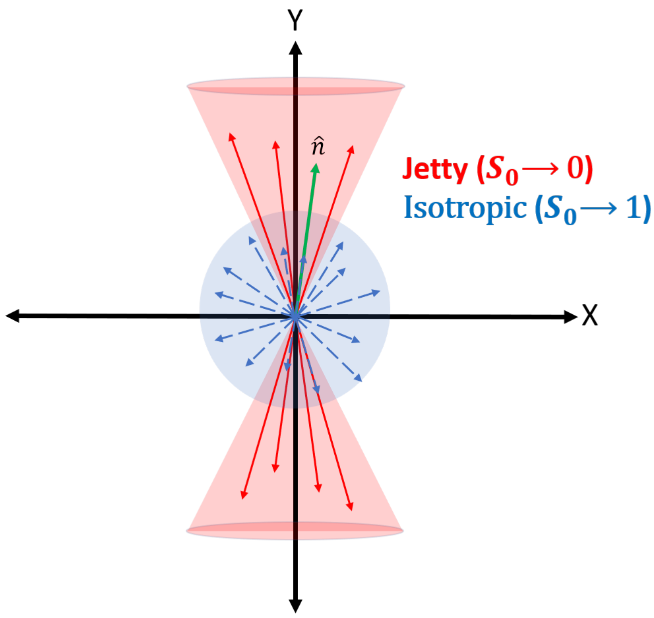

Figure 2.1: The schematic diagram of jetty and isotropic events [5].

2.1 Transverse Spherocity

Transverse spherocity allows the possibility to separate the high and low number of MPI events to isolate the behavior of particles inside jets (hard processes) and pertaining to the bulk production (soft processes).

It is defined as [7, 8, 9]:

$$S_0 = \frac{\pi^2}{4}\left|\frac{\Sigma_i\, \overrightarrow{p_{T_i}} \times \hat{n}}{\Sigma_i\, p_{T_i}}\right|^2. \tag{2.1}$$

for a unit vector $\hat{n}(n_T, 0)$ in an event, which minimizes the above ratio. The sum runs over all particles p_{T_i} in the final state, $\overrightarrow{p_{T_i}}$ represents the two momentum components transverse to the beam direction, p_{T_i} its modulus, and $\hat{n}$ is the transverse vector that minimises the sum.

By construction, the extreme limits of spherocity are related to specific configurations of events in transverse plane. The limit of spherocity is in between 0 to 1. Spherocity becoming 0 would mean that the events are pencil-like (back to back structure), while 1 would mean the events are isotropic. The pencil-like events are hard events while the isotropic events are the result of soft processes. Figure 2.1 depicts the jetty and isotropic events in the transverse plane.

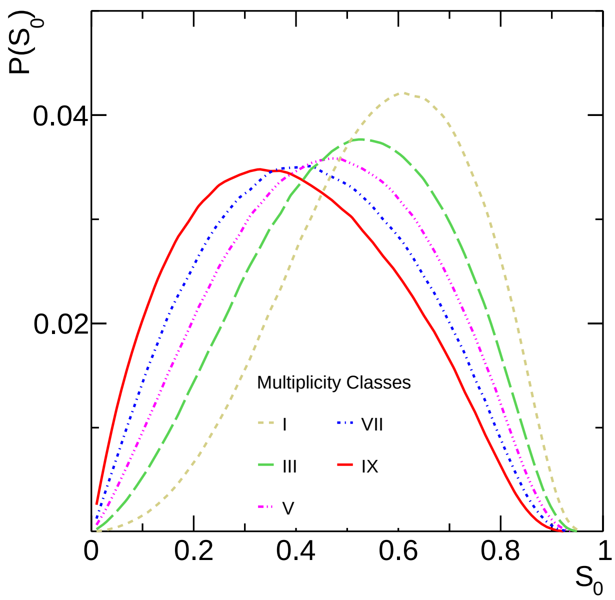

Figure 2.2: Spherocity distribution for different charged-particle multiplicity in pp-collisions at $\sqrt{s}$ = 13 TeV. Different line styles and colors are for different multiplicity classes [5].

Figure 2.2 shows the correlation between spherocity with charged-particle multiplicity. Only five alternate multiplicities are shown in figure. A clear dependence of spherocity on charged-particle multiplicity is observed. As we move from low to high-multiplicity, the peak of spherocity distribution shifts towards right. This indicates that isotropic events dominates at high-multiplicity while the low-multiplicity is dominated by jetty events.

2.2 Multi-Partonic Interactions (MPI)

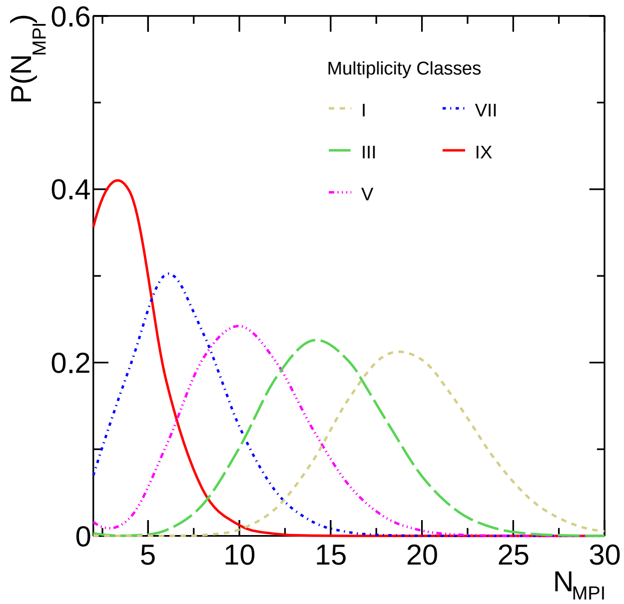

Figure 2.3: Spherocity distribution for different charged-particle multiplicity in pp-collisions at $\sqrt{s}$ = 13 TeV. Different line styles and colors are for different multiplicity classes [5].

In the framework of QCD each hadron is described as collection of elementary constituents (quarks and gluons). The interactions between these constituents belonging to different colliding hadrons are the kernel of the complicated processes which leads to the detection of new particles. The composite nature of hadrons makes possible to have multiple parton hard-scatterings i.e., events in which two or more distinct hard parton interactions occur simultaneously in a single hadron-hadron collision. Such cross-sections tend to increase with collision energy at fixed final state invariant masses. As a result, relatively low invariant masses events could receive enhanced contributions from multiple

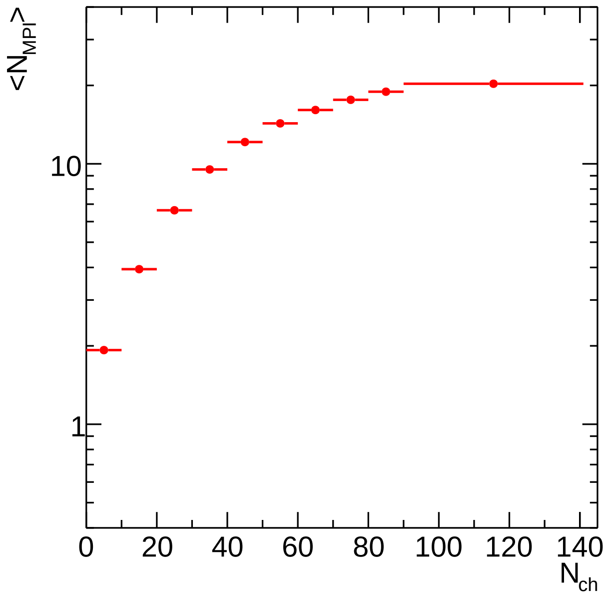

Figure 2.4: The number of MPI as a function of charged-particle multiplicity.

hard scatterings. These events are known as Multiple Parton Interactions (MPI).

The manifestation of MPI can be seen in various ways in high energy hadronic collisions. So we can expect a relation between the charged-particle multiplicity of simultaneous partonic scatterings and their typical scale. The MPI's play important role in the soft regime, characterized by small transverse momenta (p_{T}) of the produced particles. While for relatively large p_{T} values, the measurement of MPI will mostly focus on two simultaneous scatterings.

From figure 2.3 a clear dependence of MPI with charged-particle multiplicity can be observed. As we move from low to high-multiplicity the peak of MPI distribution shifts towards higher number of MPI which suggests that larger number of multi-partonic interactions occur at high-multiplicity pp-collisions. In figure 2.4 we observe the saturation of mean N$_{mpi}$ with increasing number of charged-particle multiplicity. This is an important observation as we can now treat N$_{mpi}$ and N$_{ch}$ for different scaling. Taking both N$_{mpi}$ and N$_{ch}$ will be a better criteria for the selectivity of events.

Chapter 3

Analysis Methodology

The analysis presented throughout this thesis was carried out in C++, using the framework of ROOT for data analysis. PYTHIA was used in order to generate the various particle interactions. Root was used to draw all the plots using different phase space cuts.

3.1 ROOT: Framework

ROOT is a software mainly written in object oriented C++ language integrated with other languages as Python and R. It provides all the functionality to deal with analysis of large volume of data. Facilities like storage, visualisation and plotting of data are available in ROOT. Many powerful mathematical and statistical tools are available to operate on data. The results of analysis can be displayed with scatter plots, histograms, fitting function and all these can be saved in different formats. It is an advanced Graphics User Interface (GUI).

3.2 PYTHIA: Event generator

PYTHIA is a program based on pQCD, used to simulate ultra-relativistic collision events. It is a blend of many models and theory relevant in physics like parton distributions, hard and soft interactions, initial- and final-state parton showers, fragmentation, multipartonic interactions, color reconnection and decay [10]. The main emphasis is on multi-particle production in collisions between elementary particles. Many process like hard interactions in e^+e^-, $p\bar{p}$

and $e^{-}p$ colliders can be simulated using PYTHIA although other applications are also envisaged. The program is intended to generate complete events having as much details as in experiments of LHC within the bounds of our current understanding of the underlying physics. An overview of the main physics features of PYTHIA are given in the next section.

3.3 Physics Overview in PYTHIA

All the processes given here are incorporated in PYTHIA [11].

- Hard Processes
- Resonance Decyas
- Parton Distributions
- Initial- and Final-State Radiations
- Matrix elements
- Parton Showers
- Beam Remnants and Multiple Interactions
- Hadronization
- Decays

The basis of hadronization in PYTHIA 8 is the Lund String Fragmentation Model, where the confined color field between a quark-antiquark ($q\bar{q}$) pair is designed as semi-classical string with tension κ = 1 GeV/fm.

3.4 Color Reconnection

The color reconnection allows hadronizing strings to reconnect creating quark junctions that increase hadron production. It reshuffles the colors prior to the hadronization based on three principles given below:

- Use SU(3) color rules to check the compatibility of two strings.

- It uses simple space-time picture to see whether the two strings co-exist.

- The λ string-length is minimized for the best color configuration.

The flow like effects observed in pp-collisions can be potentially connected to color reconnection. It does not requires a medium to be formed but can change the final state of the system [12].

3.5 Analysis Formalism

PYTHIA 8.235 includes multi-partonic interaction (MPI) which is crucial to explain the underlying events, multiplicity distributions and flow-like patterns in terms of color reconnection. The detailed description of the physics processes in PYTHIA 8.235 can be found in Ref. [11]. For our analysis we have implemented the inelastic, non-diffractive component of the total cross-section for all soft QCD processes using the switch (SoftQCD : all = on). This switch allows soft QCD processes to occur during pp-collisions. 250 million events were generated at beam energy $\sqrt{s} = 13$ TeV with Monash 2013 Tune (Tune:14) [13]. Different tunes are available in PYTHIA which corresponds to certain sets of parameters matched with experimetal data. The MPI based scheme of color reconnection (ColorReconnection:mode(0)) was implemented while generating data so that we allow color strings to attach befor hadronization. Final charged particles were selected in the pseudo-rapidity range of $|\eta| < 0.8$. The particle identification in pythia is done by particle identification number (PID) in the pseudo-rapidity range of $|\eta| < 0.8$.

The minimum bias events are the events where no selection on charged-particle multiplicity and spherocity is applied. For the generated events, all the hadrons were allowed to decay except the ones used in our study (Hadron-Level:Decay = on). The charged-particle multiplicities ($N_{\rm ch}$) have been chosen in the acceptance of V0 detector with pseudo-rapidity range of V0A ($2.8 < \eta < 5.1$) and V0C ($-3.7 < \eta < -1.7$) [14] in accordance with experimental conditions in ALICE. The events generated using these cuts are then further divided in ten multiplicity (V0M) bins, each bin containing 10% of total events. The table 3.1 lists all ten charged-particle multiplicities. The spherocity distribution is selected in the pseudo-rapidity range of $|\eta| < 0.8$. All events have minimum constraint of 5 charged particles with $p_{\mathrm{T}} > 0.15$ GeV/c. In the spherocity distribution the jetty events are those having $0 \leq S_0 < 0.29$ with lowest 20 percent and the isotropic events are those having $0.64 < S_0 \leq 1$ with highest 20 percent of the total events.

Table 3.1: V0M multiplicity classes and the corresponding charged-particle multiplicities

V0M class	I	II	III	IV	V	VI	VII	VIII	IX	X
N_{ch}	50-140	42-49	36-41	31-35	27-30	23-26	19-22	15-18	10-14	0-9

3.6 Thermodynamics of pp-collision

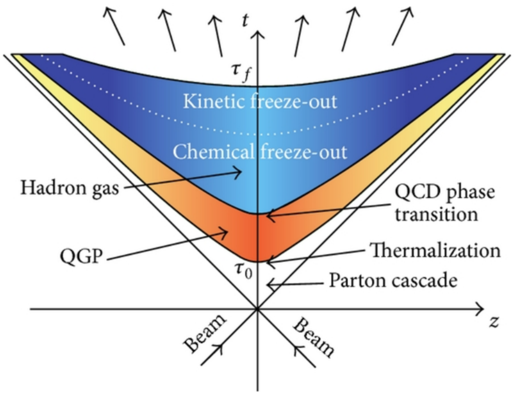

Figure 3.1: The schematic diagram for the evolution of QGP and freeze-out hyperspace.

The initial energy density in heavy ion collisions results in high pressure gradient, which leads the fireball to expand. Recent study on suppression of $\mathrm{K}^{*0}/\mathrm{K}$ as a function of charged-particle multiplicity in pp-collisions indicate the presence of hadronic phase in high-multiplicity pp-collisions at LHC energies [15]. The thermodynamic properties of QCD matter can be studied through the analysis of particle production in small systems like proton+proton. During the evolution of QCD matter, there are two types of freeze-outs: chemical and kinetic freeze-out. The hadronic phase is the state between kinetic freeze-out and chemical freeze-out. Chemical freeze-out is when inelastic scatterings stop, and the particle ratios are fixed. After chemical freeze-out the elastic scattering among the particles continues to occur which leads to the change in momentum. When the average distance between particles becomes large enough to make the elastic scattering stop, the system is said to have reached kinetic freeze-out. At this moment the transverse momentum of particles are fixed and particles stream out to reach detectors. For this reason, the study of transverse momentum spectra (p_{T}) of the produced particles can be used to determine the kinetic freeze-out temperature ($\mathrm{T_{kin}}$). The freeze-out processes are complicated in nature and may show a hierarchy. Different types of particles ceases at different time scales, which is the case in a differential freeze-out scenario.

3.6.1 Application of Tsallis Non-extensive Statistics in pp-collisions

The transverse momentum (p_T) spectra of created hadrons in high energy collisions follow a thermalised Boltzmann type of distribution as

$$E\frac{d^3\sigma}{dp^3} \simeq C\exp(\frac{p_T}{T_{kin}}) \tag{3.1}$$

where T_{kin} is the kinetic-freeze-out temperature.

But the identified particle p_{T}-spectra do not follow Boltzmann-Gibbs distribution due to possible pQCD contributions at higher energies. To take care of pQCD contribution empirically, a power law in p_T has been proposed [16]. To explain the experimental data over a wide range of p_T both these aspects were combined by Hagedron [17] and is given by

$$E\frac{d^3\sigma}{dp^3} \simeq C\left(1+\frac{p_T}{p_0}\right)^{-n} \rightarrow \begin{cases} \exp\left(-\frac{np_T}{p_0}\right) & for\ p_T \rightarrow 0, \\ \left(\frac{p_0}{p_T}\right)^n & for\ p_T \rightarrow \infty, \end{cases} \tag{3.2}$$

where $C,\ p_0$ and n are fitting parameters. This function behaves as exponential function for lower p_T whereas for higher p_T it behaves as power law. A deviation was observed by experiments while describing the p_T spectra of identified particles using the equilibrium statistical distribution function at RHIC [18, 19] and LHC [20, 21, 22, 23]. The $\langle p_T \rangle$ (mean transverse momentum) is associated with the temperature of hadronic matter but if the systems are far away from thermal equilibrium one fails to explain its behaviour. In systems far away from thermal equilibrium, the temperature fluctuates either event-by-event or within the same event. This requires the use of non-extensive Tsallis statistics for complete description of p_T spectra in high energy collisions. A thermodynamically consistent Tsallis's modified form of non-extensive distribution function at mid-rapidity (y) is given by,

$$\frac{1}{p_T}\frac{d^2N}{dp_T dy}\bigg|_{y=0} = \frac{gVm_T}{(2\pi)^2}\left[1+(q-1)\frac{m_T}{T}\right]^{-\frac{q}{q-1}}. \quad (3.3)$$

where, g is the degeneracy factor, V is the system volume, $m_{\rm T} = \sqrt{p_T^2+m^2}$ is the transverse mass and q is the non-extensive parameter, which is the measure of degree of deviation from equilibrium. In the limit of $q \to 1$, the standard Boltzmann-Gibbs distribution (Eq.(3.1)) is recovered from Tsallis distribution (Eq.(3.3))

We fit $p_{\rm T}$-spectra with Eq. 3.3 for all particles to obtain the mass dependent temperature like parameter T and non-extensive parameter, q. We study these parameters as a function of spherocity and charged-particle multiplicity.

3.6.2 Boltzmann Gibbs Blastwave Model (BGBW)

The low p_T region of transverse momentum spectra in high-multiplicity classes in pp-collisions is explained by incorporating radial flow (β) into Boltzmann-Gibbs distribution function. This is referred by Boltzmann-Gibbs Blast Wave (BGBW) model. The particles are boosted by radial flow (β) in the system. We can extract T_{kin} and radial flow (β) by fitting the identified particle transverse momentum spectra at low p_T. The invariant yield in the framework of BGBW is given as follows [24]:

$$E\frac{d^3N}{dp^3} = D\int d^3\sigma_\mu p^\mu exp(-\frac{p^\mu u_\mu}{T}), \quad (3.4)$$

where the particle four-momentum is,

$$p^\mu = (m_T\text{coshy},\ p_T\cos\phi,\ p_T\sin\phi,\ m_T\text{sinhy}), \quad (3.5)$$

the four-velocity is given by,

$$u^\mu = \cosh\rho\,(\cosh\eta,\ \tanh\rho\ \cos\phi_r,\ \tanh\rho\ \sin\ \phi_r,\ \sinh\ \eta), \quad (3.6)$$

while the kinetic freeze-out surface is parametrised as,

$$d^3\sigma_\mu = (\cosh\eta,\ 0,\ 0, -\sinh\eta)\,\tau\, r\, dr\, d\eta\, d\phi_r. \quad (3.7)$$

Here, η is the space-time rapidity. With simplification assuming Bjorken correlation in rapidity $i.e.$, $y = \eta$, Eq. 3.4 can be expressed as:

$$\left.\frac{d^2N}{dp_T dy}\right|_{y=0} = D \int_0^{R_0} r\ dr\ K_1\left(\frac{m_T\ \cosh\rho}{T_{kin}}\right) I_0\left(\frac{p_T\ \sinh\rho}{T_{kin}}\right), \tag{3.8}$$

where D is the normalisation constant. Here g is the degeneracy factor and $m_\mathrm{T} = \sqrt{p_T^2 + m^2}$ is the transverse mass.

$K_1(\frac{m_T\ \cosh\rho}{T_{kin}})$ and $I_0(\frac{p_T\ \sinh\rho}{T_{kin}})$ are the modified Bessel's functions and are given by,

$$K_1(\frac{m_T\ \cosh\rho}{T}) = \int_0^\infty \cosh y\ \exp(-\frac{m_T\ \cosh y\ \cosh\rho}{T_{kin}})dy, \tag{3.9}$$

$$I_0\left(\frac{p_T\ \sinh\rho}{T}\right) = \frac{1}{2\pi}\int_0^{2\pi} exp\left(\frac{p_T\ \sinh\rho\ \cos\phi}{T_{kin}}\right)d\phi, \tag{3.10}$$

where ρ is a parameter given by $\rho = \tanh^{-1}\beta$, with $\beta = \beta_s\ (\xi)^n$ [25, 24, 26, 27] is the radial flow. β_s is the maximum surface velocity and $\xi = (r/R_0)$, where r is the radial distance. The particles closer to the center of the fireball in the blast-wave model move slower than the particles at the edges. The average of the transverse velocity can be evaluated as [28],

$$< \beta > = \frac{\int \beta_s \xi^n \xi\ d\xi}{\int \xi\ d\xi} = (\frac{2}{2+n})\beta_s. \tag{3.11}$$

We use a linear velocity profile in our calculations i.e., ($n = 1$) and R_0 is the maximum radius of the expanding source at freeze-out ($0 < \xi < 1$).

We fit p_T-spectra with equation 3.8 for all particles to obtain the thermodynamical parameters $\mathrm{T_{kin}}$ and β parameter in every multiplicity classes. Then we study these parameters as a function of spherocity.

In the next chapter all the results from this analysis are given and discussed.

Chapter 4

Results and Discussion

As discussed in the previous chapters we have used spherocity as a tool to disentangle the jetty and isotropic events for each multiplicity class. In our analysis we study the p_T-spectra for $\pi^+ + \pi^-$, $K^+ + K^-$, p+$\bar{p}$ and $\Lambda^0 + \bar{\Lambda}^0$ as a function of spherocity and charged-particle multiplicity. We also study the thermodynamics of different spherocity classes as a function of multiplicity classes. The thermodynamic parameters obtained are studied as a function of spherocity and charged-particle multiplicity [5]. In the next sections we shall discuss the results.

4.1 p_{T}-spectra

Figure. 4.1 shows the p_{T}-spectra for pion, kaon, proton and lambda at mid-rapidity ($|\eta|< 0.5$) for different multiplicity classes in pp-collisions at $\sqrt{s}$ = 13 TeV. We observe a clear multiplicity dependence of the p_{T}-spectra for all particles. As we move from low to high charged-particle multiplicity, we observe hardening of spectral shape while the bulk production is similar for all the multiplicity classes. This trend is similar to the trend in experimental data from ALICE [29] for multiplicity dependence study in pp-collisions at $\sqrt{s}$ = 7 TeV.

Upper panel of Fig. 4.2 shows the spherocity dependence of p_{T}-spectra of identified particles for minimum bias pp-collision events. While, lower panel shows the ratio of p_{T}-spectra for isotropic and jetty events to the spherocity integrated events. We observe the crossing of the ratios for pions, kaons and protons

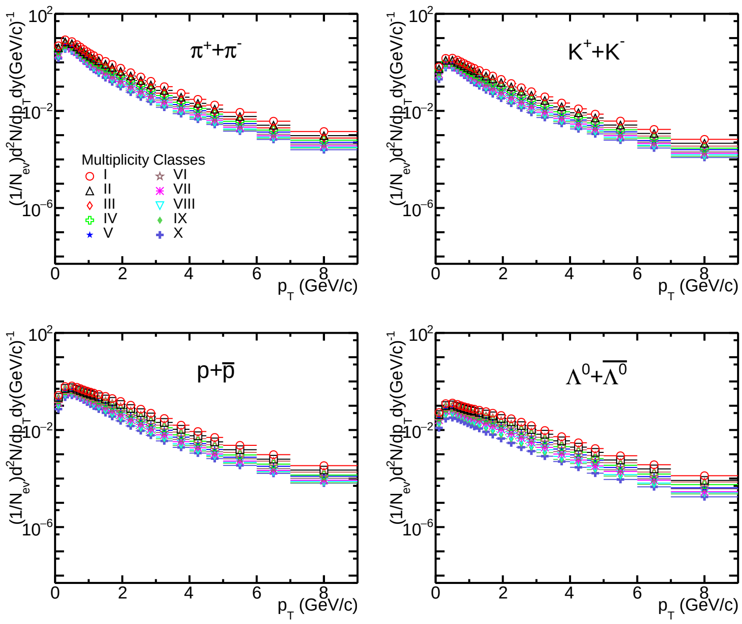

Figure 4.1: p_{T}-spectra for light-flavor hadrons like pion, kaon, proton and lambda at mid-rapidity ($|\eta| < 0.5$) as a function of charged-particle multiplicity for pp-collisions at $\sqrt{s} = 13$ TeV [5].

at around 3 GeV/c while for lambda we observe the crossing of ratio around 6 GeV/c. This indicates that for minimum bias pp-collisions, the production of pions, kaons and protons at low p_{T} are dominated by isotropic events while after 3 GeV/c, the production is dominated by jetty events. For heavier particle like Λ, the production is dominated by isotropic events till 6 GeV/c. This indicates different production mechanisms for heavier particles compared to lighter particles. This needs a further investigation with different kinds of particles.

Figure 4.3 shows the ratio of p_{T}-spectra for jetty and isotropic events to the spherocity integrated events for V0M-I (upper) and V0M-X (lower) multiplicity classes. The comparison between lowest (V0M-X) and the highest (V0M-I) multiplicity classes is done to see the effect of multiplicity on the crossing point of jetty and isotropic events. For stable particles like, π, K and p, the crossing point moves towards high-p_{T}, while going from low ($\sim$ 1 GeV/c) to high-multiplicity classes ($\sim$ 3 GeV/c). This indicates that particle production in high-multiplicity collisions are dominated by isotropic events whereas in low-multiplicity it is dominated by jetty events. The preliminary results from ALICE [30] shows a mass dependence of the crossing points for high-multiplicity

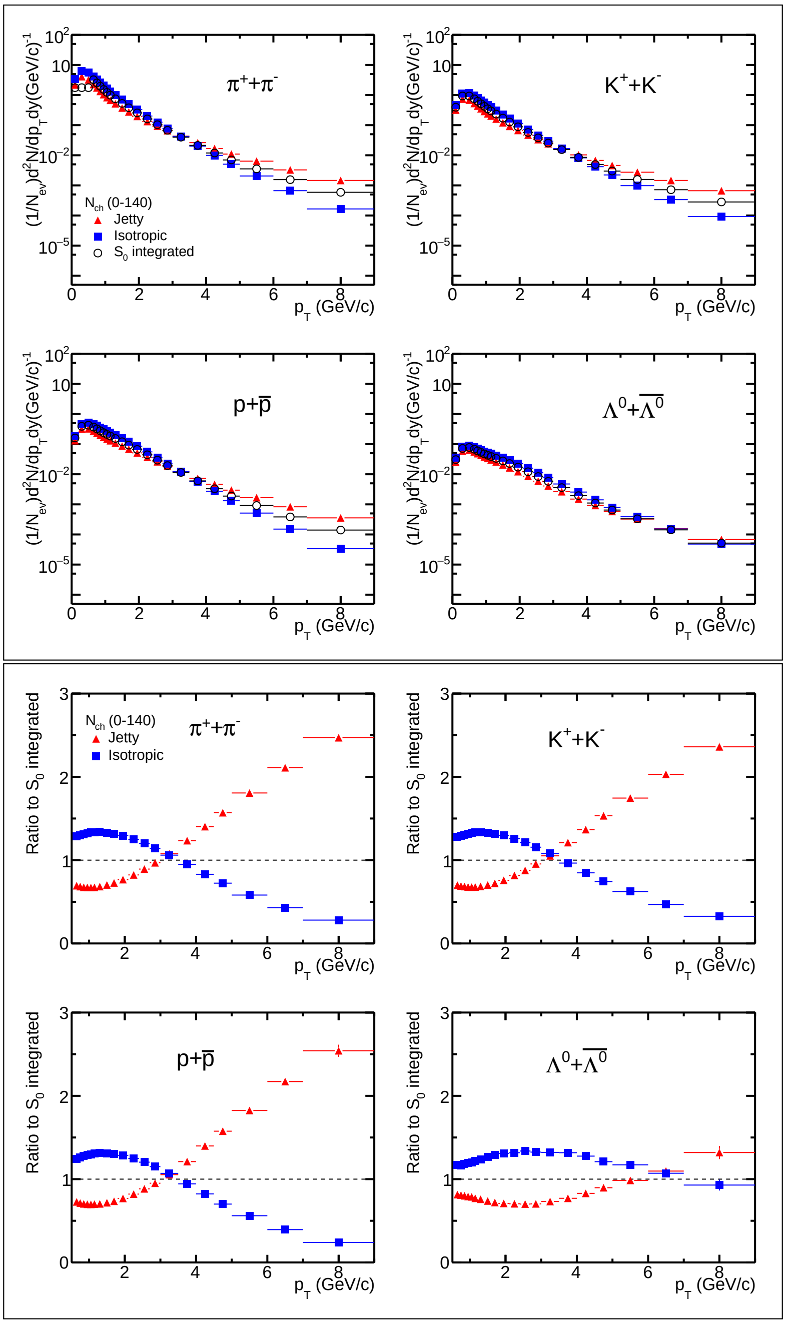

Figure 4.2: Upper Panel: p_T-spectra for pion, kaon, proton and lambda for minimum bias pp-collisions as a function of spherocity. Lower Panel: Ratio of p_T-spectra for isotropic and jetty events to the spherocity integrated events [5].

pp-collisions which could be attributed to flow-like behavior. Although the color reconnection in PYTHIA mimics a flow-like behavior [12], we do not observe mass dependence of crossing points with the default color reconnection setting. Similarly, we observe crossing points for Λ at higher-p_T (around 5 GeV/c) for V0M-I class. However, we observe the crossing point for low-multiplicity pp-collisions (V0M-X class) is similar for all particles, i.e. around 1 GeV/c.

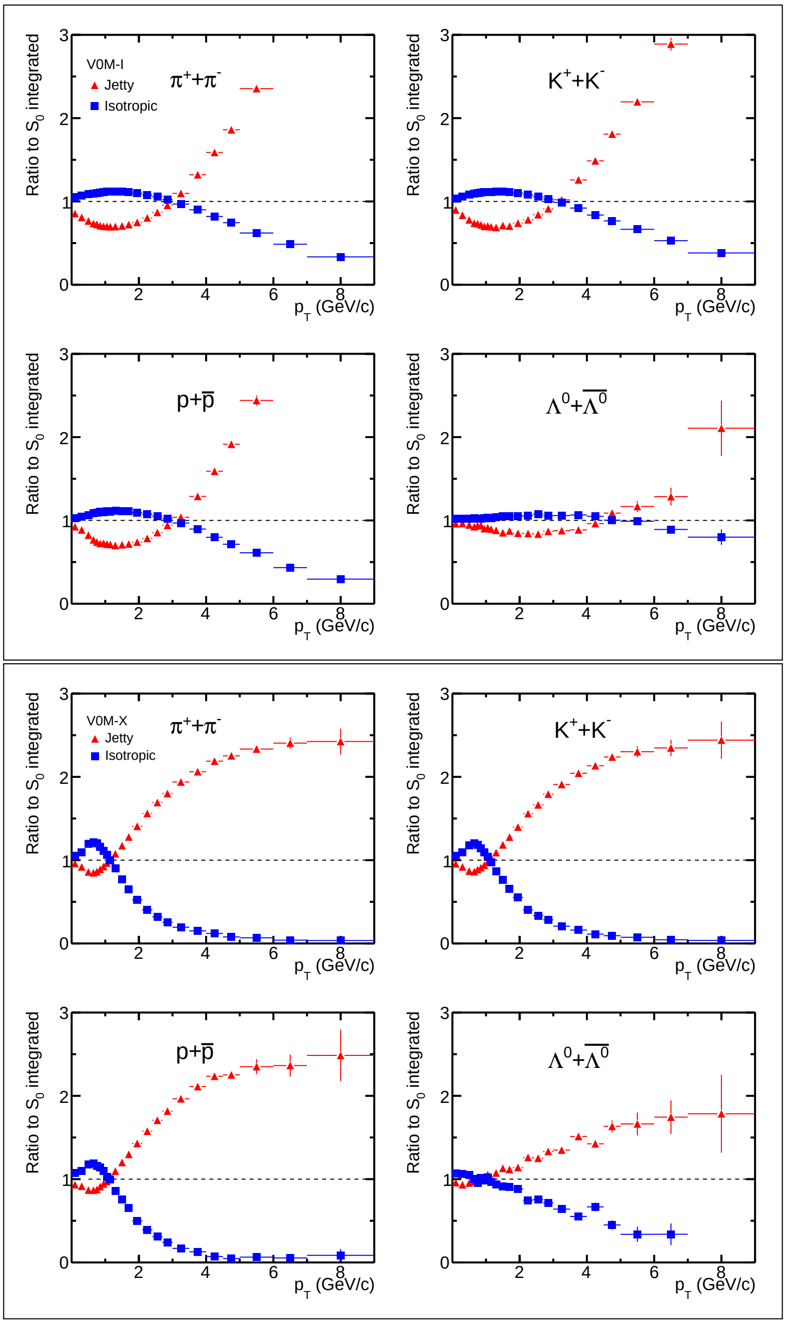

Figure 4.3: Ratio of p_{T}-spectra for isotropic and jetty events to the spherocity integrated events for V0M-I (Upper) and V0M-X (Lower) multiplicity class [5].

4.2 p_{T}-spectra: using Tsallis non-extensive statistics

We successfully fitted the p_{T}-spectra with tsallis distribution function (Eq. 4.4) and the figures 4.4, 4.5 show the fitting of p_{T}-spectra of pions, kaons, protons and lambda as a function of charged-particle multiplicity for spherocity-integrated,

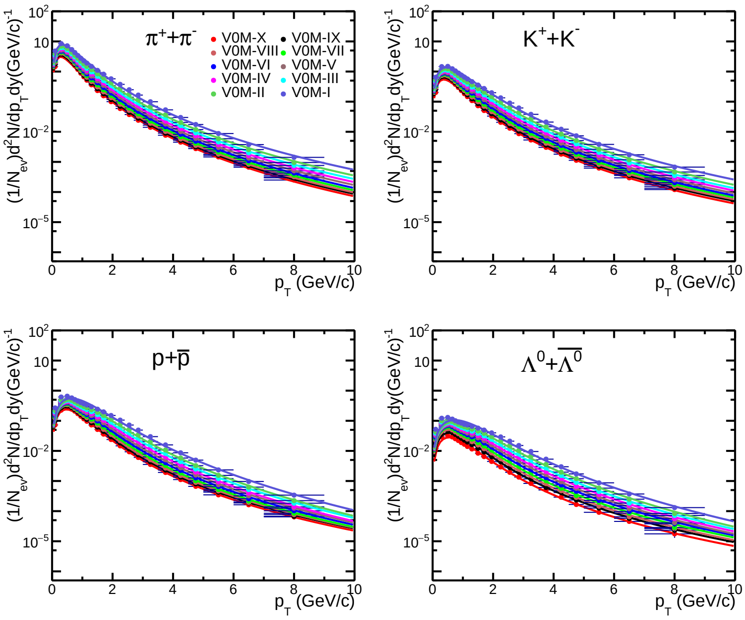

Figure 4.4: Fitting of generated p_{T}-spectra of identified hadrons using Tsallis distribution for spherocity integrated events in various multiplicity classes as shown in Table 3.1 [6].

isotropic and jetty events, respectively. We observe that the Tsallis distribution fits the generated data till $p_{\mathrm{T}} \simeq 10$ GeV/c. Figure 4.6 shows the quality of fitting in terms of the χ^2/NDF as a function of multiplicity for different spherocity classes. The values of χ^2/NDF shows that the quality of fitting is reasonably good for all the spherocity and multiplicity classes.

4.3 T_{kin}, q v/s charged-particle multiplicity

Figures 4.7 and 4.8 shows the extracted thermodynamical consistent parameters from the fitting of p_{T}-spectra using Tsallis distribution Eq. 3.3 as a function of charged-particle multiplicity for different spherocity classes. Figure 4.7 shows that the temperature parameter increases with charged-particle multiplicity for spherocity-integrated and isotropic events. But the jetty events seem to show a reverse trend for pions, kaons and protons. For lambda the temperature parameter shows an increase with multiplicity for jetty events. For all instances, the temperature for jetty events is lower compared to the other spherocity classes. We also observe that the temperature for lighter particles does not change signif-

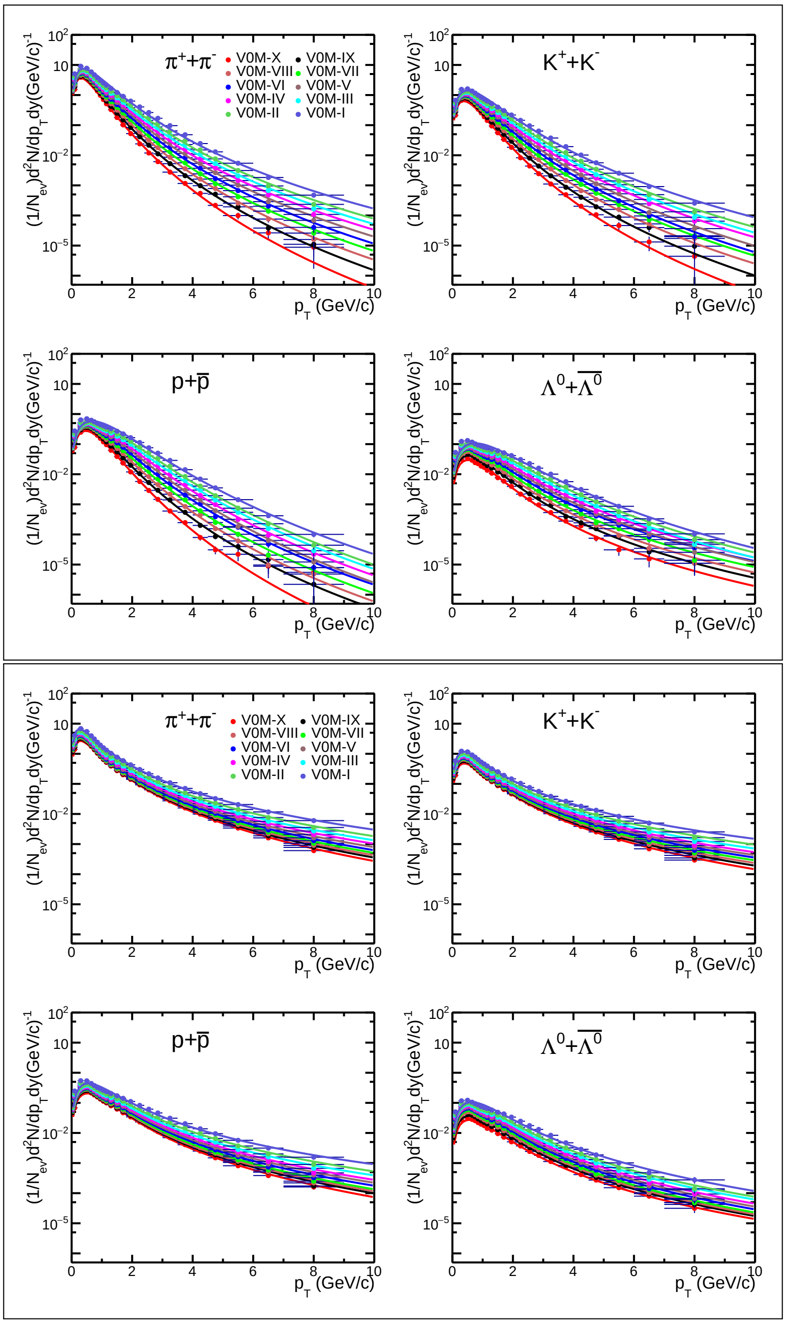

Figure 4.5: Fitting of generated p_{T}-spectra of identified hadrons using Tsallis distribution for isotropic (Upper) and jetty (Lower) events in various multiplicity classes as shown in Table 3.1 [6].

icantly with multiplicity while with increase in mass, the temperature increases steeply as a function of multiplicity. Figure 4.8 shows that for isotropic events, the non-extensive parameter, q values remain lower compared to the spherocity-integrated events which suggests that isotropic events have got a higher degree of equilibration compared to spherocity-integrated events. This indicates that while studying the QGP-like conditions in small systems, one should separate

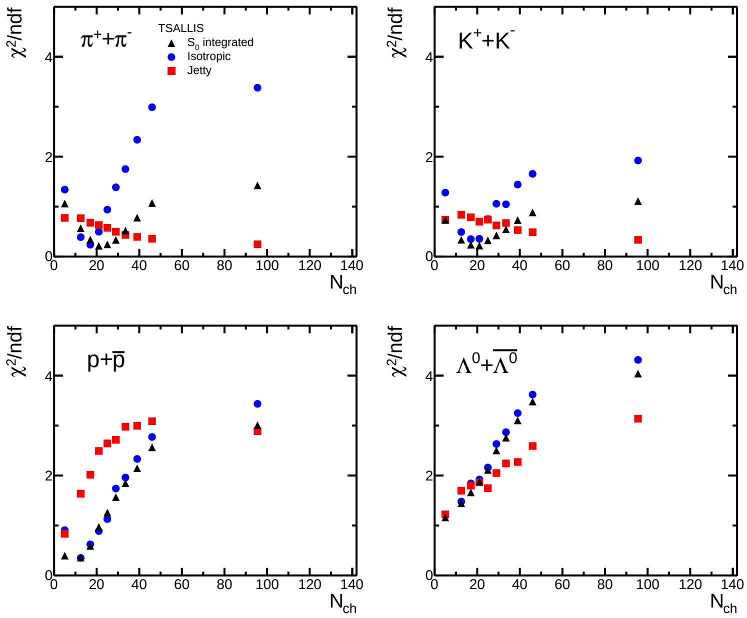

Figure 4.6: χ^2/NDF for the fitting of generated p_T-spectra of identified hadrons using Tsallis distribution in different spherocity and multiplicity classes [6].

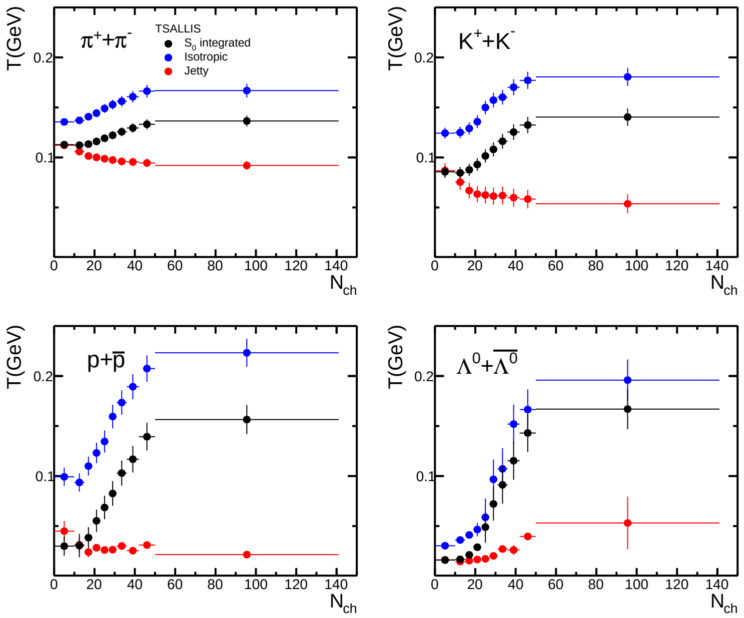

Figure 4.7: Multiplicity dependence of T in different spherocity classes from the fitting of Tsallis distribution using Eq. 3.3 [6].

the isotropic events from the spherocity-integrated events, as the production dynamics are different. On the contrary, the q value for jetty are always higher compared to spherocity-integrated events indicating that the jetty events remain far away from equilibrium. The present study is very useful in understanding the

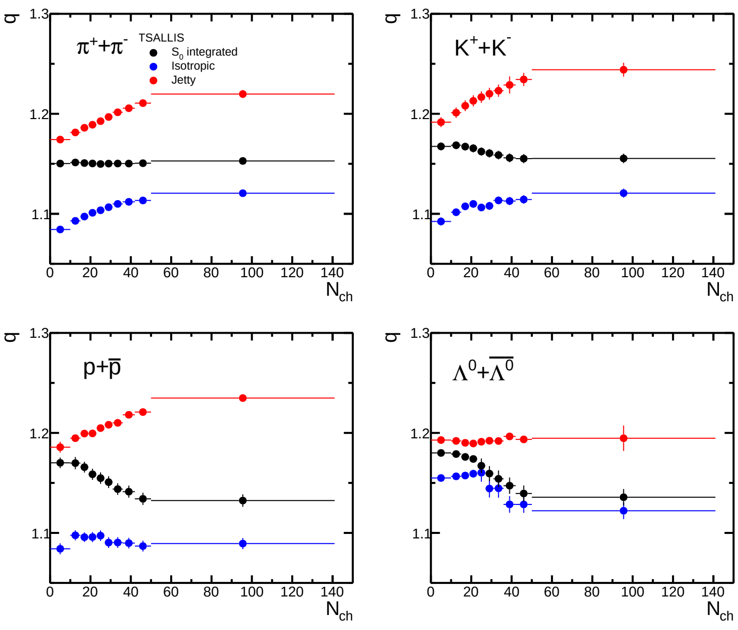

Figure 4.8: Multiplicity dependence of q in different spherocity classes from the fitting of Tsallis distribution using Eq. 3.3 [6].

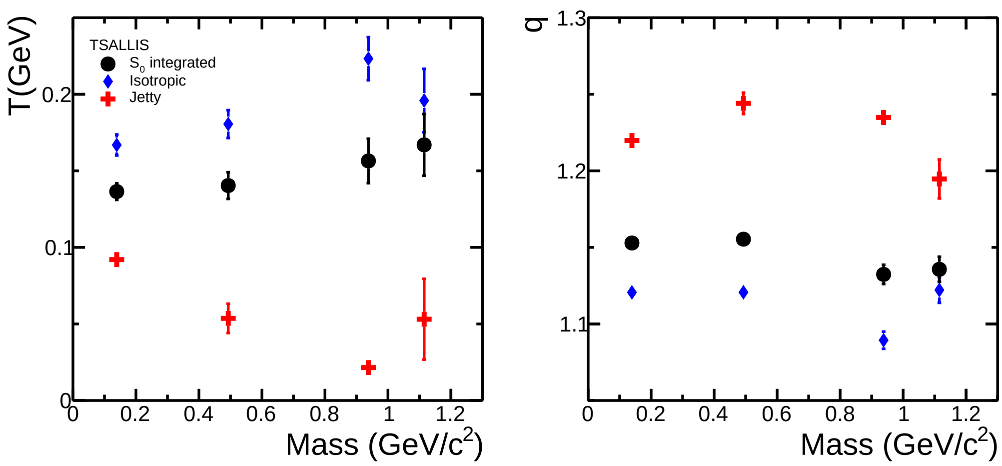

Figure 4.9: Mass dependence of T and q in different spherocity classes for the highest multiplicity class using Tsallis distribution fit (Eq. 3.3) [6].

microscopic features of degrees of equilibration and their dependencies on the number of particles in the system and on the geometrical shape of an event. Now the mass dependence of these thermodynamic parameters would be interesting to study. To do so, we have picked the events with highest multiplicity class and done the same spherocity analysis taking different particles as discussed here, which is shown in Fig. 4.9. The temperature remains higher for particles with higher masses for all the spherocity classes in high-multiplicity pp-collisions, this is an indication of differential freeze-out scenario. This suggests that lighter particles freeze-out later and massive particles freeze-out early in the system. However, the jetty events show a reverse trend.

To explore the flow-like features in small systems, we needs to focus on the low-p_{T} of the particle spectra with Boltzmann-Gibbs Blastwave (BGBW) model, the results of which are discussed in next sub-section. As we saw an indication of a differential freeze-out scenario, in the following section we consider making individual spectral analysis using BGBW, instead of a simultaneous fitting, which is usually necessitated by a single freeze-out scenario.

4.4 p_{T}-spectra: using Boltzmann-Gibbs Blastwave Model

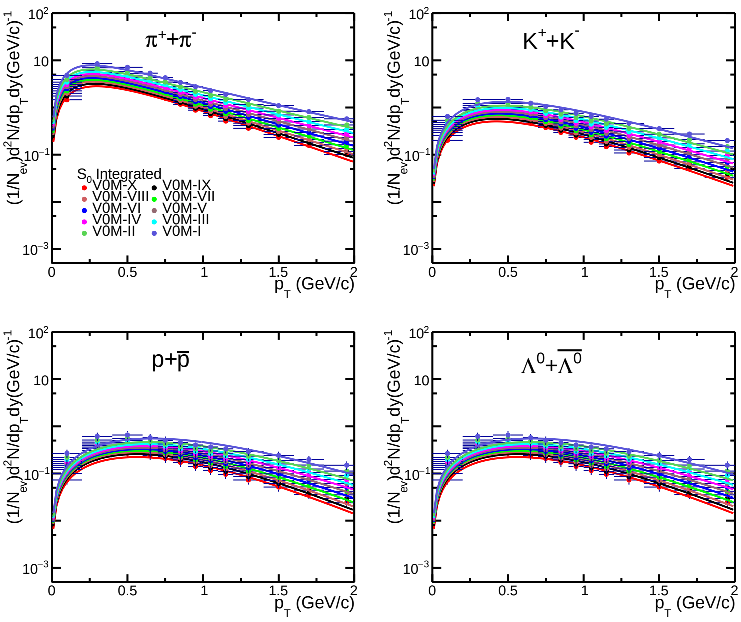

Figure 4.10: Fitting of generated p_{T}-spectra of identified hadrons using BGBW model for spherocity integrated events in various multiplicity classes as shown in Table 3.1 [6].

In the BGBW model, the particles closer to the center of the fireball move slower than the ones at the edges. In our calculation, for the sake of simplicity we use a linear velocity profile i.e. $n = 1$. Figures 4.10 and 4.11 display the fitting of p_{T}-spectra for pions, kaons, protons and lambda as a function of charged-particle

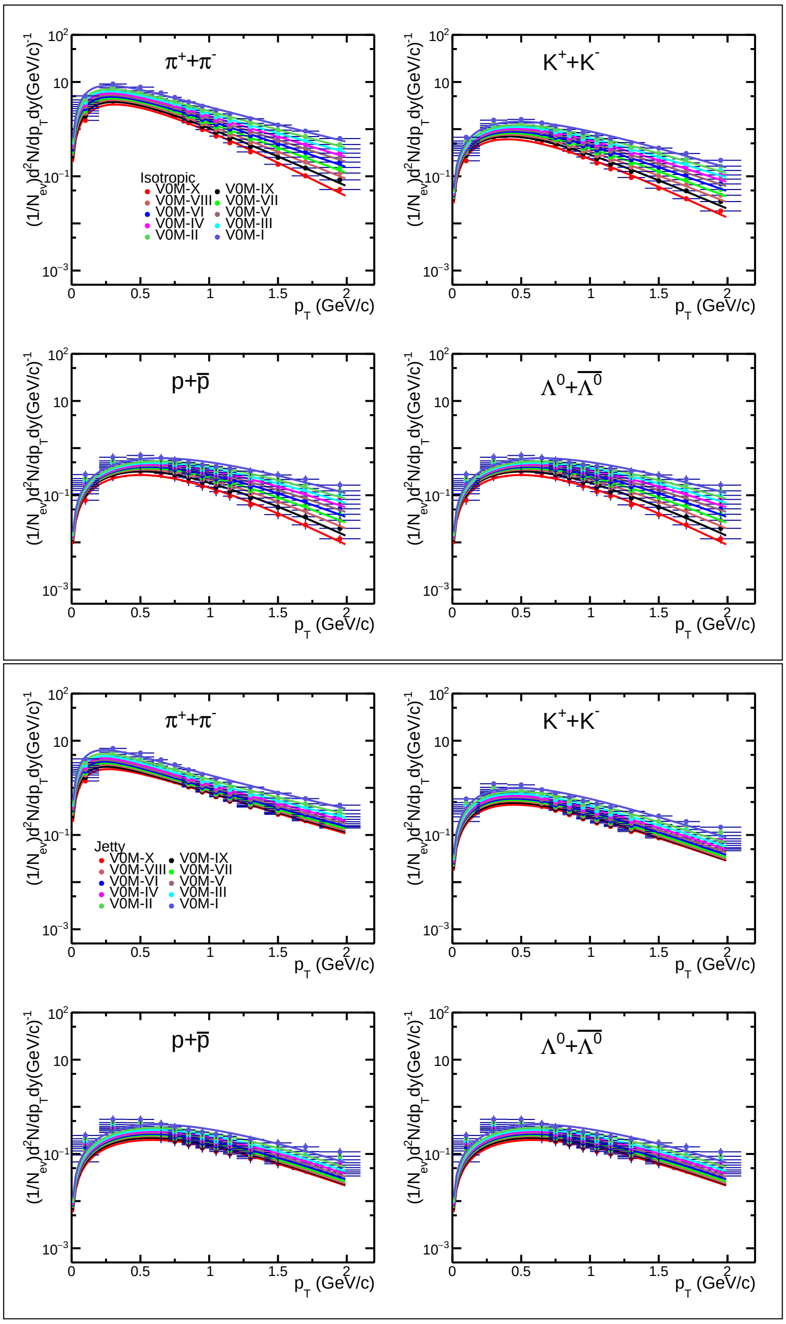

Figure 4.11: Fitting of generated p_{T}-spectra of identified hadrons using BGBW model for isotropic (Upper) and jetty (Lower) events in various multiplicity classes as shown in Table 3.1 [6].

multiplicity using BGBW distribution using Eq. 3.4 for spherocity-integrated, isotropic and jetty events, respectively. The BGBW distribution fits the spectra for all identified hadrons till $p_{\mathrm{T}} \simeq 2$ GeV/c. Figure 4.12 shows the χ^2/NDF for the fitting of generated p_{T}-spectra using BGBW model in different charged-particle multiplicity and spherocity classes. Pions are better describes by the BGBW model as the χ^2/NDF for pion is relatively lower compared to kaons

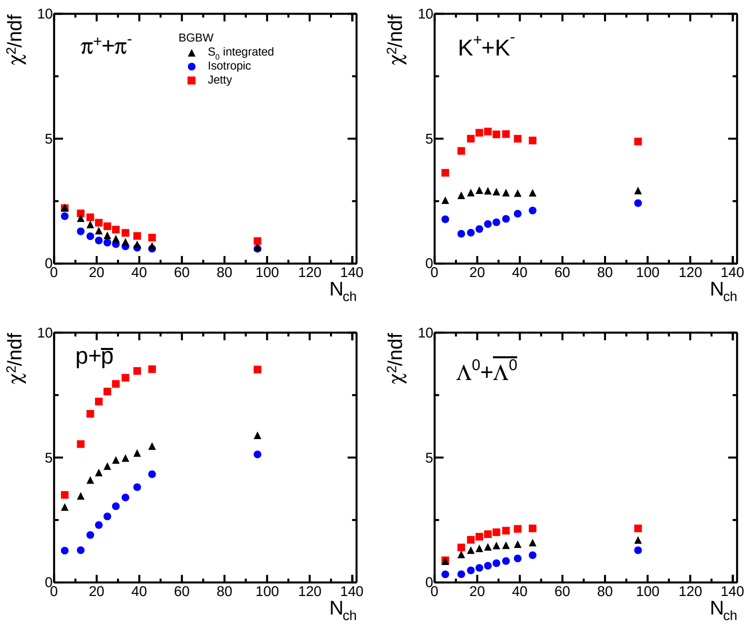

Figure 4.12: χ^2/NDF for the fitting of generated $p_{\rm T}$-spectra of identified hadrons using BGBW model in different spherocity and multiplicity classes [6].

and protons. The higher value of χ^2/NDF for pions in low-multiplicity is due to the fact that the number of particles is less in the lower multiplicity classes which makes the fitting worse. But as we move from low to high-multiplicity the fitting gets better and we see decrease in the value of χ^2/NDF. The fitting for jetty events are worse compared to isotropic and spherocity-integrated events as expected, indicating that the jetty events remain far from equilibrium and a BGBW description becomes less significant.

Since BGBW analysis is in the soft sector of particle production, it is interesting to note that we do not see any difference between jetty, isotropic and spherocity integrated events so far the multiplicity dependence of kinetic freeze-out temperature and the radial flow velocity are concerned, except pions.

4.5 T_{kin}, β v/s charged-particle multiplicity

In figs. 4.13 and 4.14 for all the identified particles, the kinetic freeze-out temperature shows a linear increase with final state multiplicity except for pions. The radial flow velocity also shows a uniform increase with multiplicity classes for all the particles. We now take the highest multiplicity class to look into the

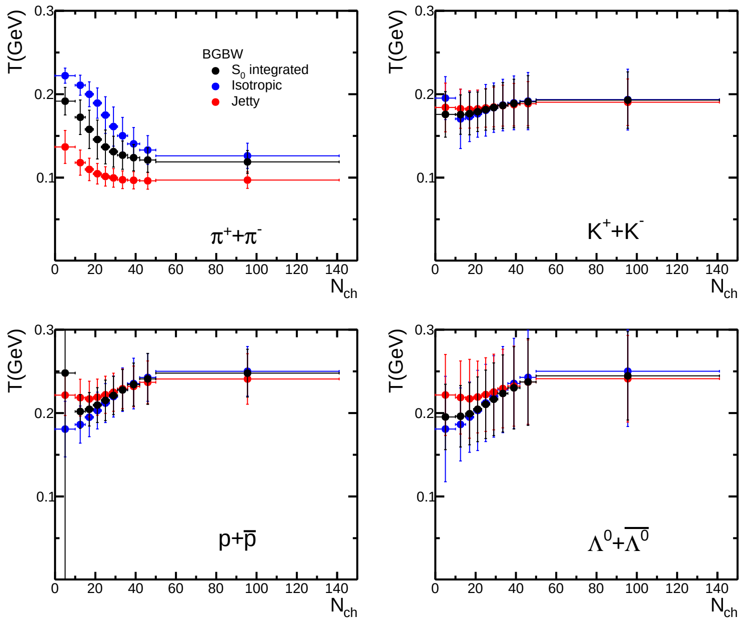

Figure 4.13: Multiplicity dependence of T in different spherocity classes from the fitting of BGBW model [6].

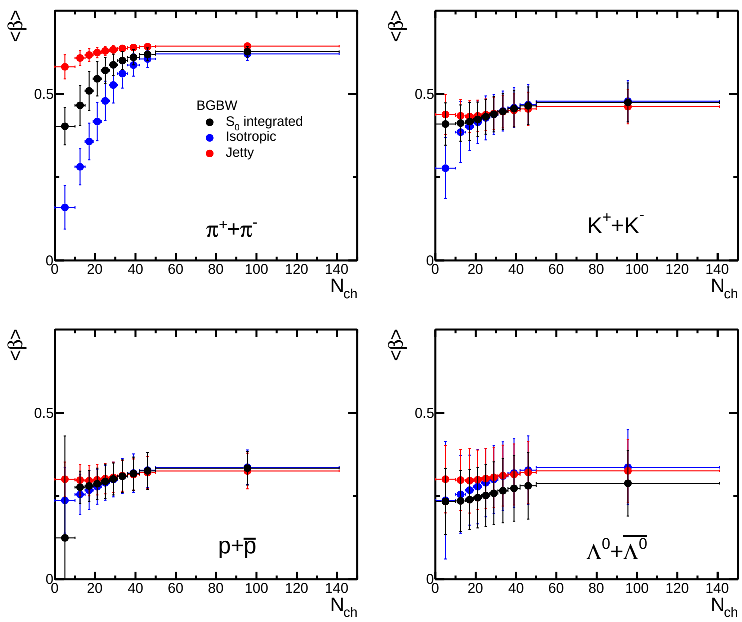

Figure 4.14: Multiplicity dependence of $< \beta >$ in different spherocity classes from the fitting of BGBW model [6].

particle mass dependence of the freeze-out parameters. Figure 4.15 shows that the temperature increases with mass for the highest multiplicity pp-collisions consisted with the Tsallis distribution from previous section, indicating a differential freeze-out scenario. The temperature from BGBW model also suggests

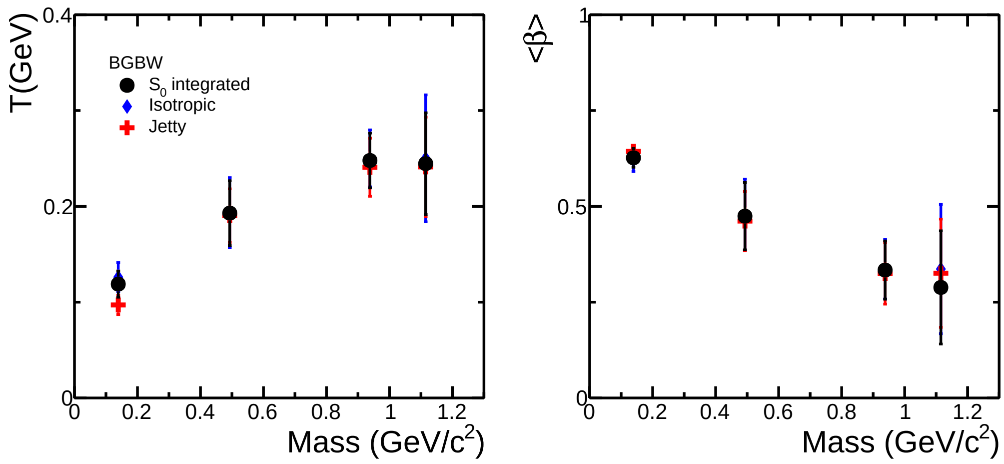

Figure 4.15: Mass dependence of T and $<\beta>$ in different spherocity classes for the highest multiplicity class using BGBW fit up to $p_{\mathrm{T}} \sim 2$ GeV/c [6].

that the particles with heavier mass freeze-out early in time. We observe a decrease in the radial flow velocity with increasing particle mass, which supports a collective behaviour. We observe $<\beta> \simeq 0.62$ for pions and $<\beta> \simeq 0.31$ for lambda.

Having discussion on all the results obtained from our analysis now we conclude our work with important findings in the next chapter.

Chapter 5

Conclusion and Outlook

In this thesis we have made an extensive study of several observables taking spherocity and charged-particle multiplicity in pp-collisions at $\sqrt{s}$ = 13 TeV using PYTHIA 8. We also performed a double differential study of the identified particle spectra and the system thermodynamics as a function of charged-particle multiplicity and spherocity. This helps us to understand the underlying event dynamics of pp-collisions and the possible differences/similarities in freeze-out parameters when pp-collision is compared to heavy ion collision. The aim of this analysis is to understand the high-multiplicity pp events at the LHC energies in view of medium formation in pp-collisions. The MPI and CR effects responsible for particle production were invoked in our study and then transverse spherocity was used to understand various aspects of particle production in pp-collisions.

The findings of this thesis are summarised as below :

1. We study the event shape dependence of the transverse momentum (p_{T}) spectra of identified particles. We observe a clear spherocity dependence of p_{T}-spectra for all particles.

2. While taking the ratio of jetty and isotropic events to spherocity integrated events we observe a crossing point. The crossing point suggests the dominance of different events in different p_{T} regime. Before the crossing point isotropic events are dominant while as we go towards higher momentum regime jetty events take over isotropic ones.

3. The crossing of ratios is observed to be charged-particle multiplicity dependent. As we go from low to high-multiplicity the crossing point shift

towards higher p_{T} value which suggests that at high-multiplicity isotropic events have more dominance over jetty events.

4. In the thermodynamic study we observe the dependence of parameters obtained by fitting the full range of p_{T}-spectra using Tsallis distribution function and the Blastwave function was fitted till 2GeV/c^2 of p_{T}-spectra.

5. The parameters like $\mathrm{T_{kin}}$, β, q were obtained successfully.

6. A clear spherocity dependence is observed for temperature and with increasing multiplicity temperature also increases for all particles. For higher mass particles the increase in temperature is more steeper with increasing multiplicity.

7. The non-extensive parameter q was studied and found to be spherocity and multiplicity dependence. Also the q value for jetty events were larger than isotropic events, which suggests that jetty events have a tendency to stay away from equilibrium and isotropic events approach towards equilibrium compared to spherocity integrated events.

8. As we go from low to high mass particle for highest multiplicity the temperature is also increasing which is an indication of differential freeze-out.

9. The radial flow velocity is found to be mass dependent. As we go from low mass to high mass radial flow velocity is decreasing, which is an indication of a hydronamic behaviour. This indicates collectivity in high-multiplicity pp-collisions at the LHC energies.

Recent findings in high-multiplicity pp-collisions opened a new domain and many challenges to explore. The collective behaviour, strangeness enhancement, ridge structure in high-multiplicity needs a proper investigation in data as well as models like PYTHIA, DYPSY. Event shape study allows us to get more information by separating different geometric events like jetty and isotropic. These results can help us to understand LHC pp-collisions in a deeper way.

Appendix A

Thermodynamic consistency of Tsallis Statistics

From the first and second law of thermodynamics we have

$$d\epsilon = Tds + \mu dn, \tag{A.1}$$

$$dP = sdT + nd\mu. \tag{A.2}$$

here $\epsilon = E/V, s = S/V$ and $n = N/V$ are the energy, entropy and particle number densities respectively.

For the thermodynamic consistency, the following relations need to be satisfied.

$$T = \frac{\partial \epsilon}{\partial s}\Big|_n, \tag{A.3}$$

$$\mu = \frac{\partial \epsilon}{\partial n}\Big|_s, \tag{A.4}$$

$$n = \frac{\partial \epsilon}{\partial \mu}\Big|_T, \tag{A.5}$$

$$s = \frac{\partial \epsilon}{\partial T}\Big|_\mu \tag{A.6}$$

From the first law of thermodynamics

$$P = \frac{-E + TS + \mu N}{V} \tag{A.7}$$

we will take the partial derivative of the above equation with respect to μ, which will lead us to:

$$\frac{\partial P}{\partial \mu}\Big|_T = \tfrac{1}{V}\left[-\tfrac{\partial E}{\partial \mu} + T\tfrac{\partial S}{\partial \mu} + N + \mu\tfrac{\partial N}{\partial \mu}\right], \tag{A.8}$$

$$= \tfrac{1}{V}\Big[N + \textstyle\sum_i -\tfrac{T}{q-1}\Big(1 + (q-1) \tag{A.9}$$

$$\tfrac{E_i-\mu}{T}\Big)\tfrac{\partial n_i^q}{\partial \mu} + \tfrac{Tq(1-n_i)^{q-1}}{q-1}\tfrac{\partial n_i}{\partial \mu}\Big], \tag{A.10}$$

by explicit calculations

$$\frac{\partial n_i^q}{\partial \mu} = \frac{q n_i^{q+1}}{T} \left[1 + (q-1)\frac{E_i - \mu}{T}\right]^{-1+\frac{1}{1-q}}, \tag{A.11}$$

$$\frac{\partial n_i}{\partial \mu} = \frac{n_i^2}{T} \left[1 + (q-1)\frac{E_i - \mu}{T}\right]^{-1+\frac{1}{1-q}}, \tag{A.12}$$

and

$$(1 - n_i)^{q-1} = n_i^{q-1} \left[1 + \frac{(q-1)(E_i - \mu)}{T}\right] \tag{A.13}$$

substituting the above in Eq. A.10 we get

$$\frac{\partial P}{\partial \mu}\Big|_T = n \tag{A.14}$$

This proves the thermodynamical consistency.

Bibliography

[1] S. Zhang, L. Zhou, Y. Zhang, M. Zhang, C. Li, M. Shao, Y. Sun and Z. Tang, Nucl. Sci. Tech. **29** (2018) 9, 136, arXiv:1803.05767 [hep-ph].

[2] J. Adam *et al.* [ALICE Collaboration], Nature Phys. **13**, 535 (2017).

[3] ATLAS Physics website, https://atlas.cern/discover/physics.

[4] Raghunath Sahoo, arXiv:1604.02651v1 [nucl-ex] .

[5] A. Khuntia, S. Tripathy, A. Bisht and R. Sahoo, arXiv:1811.04213 [hep-ph].

[6] S. Tripathy, A. Bisht, R. Sahoo, A. Khuntia and M. Salwan, arxiv:1905.07418 [hep-ph].

[7] E. Cuautle, R. Jimenez, I. Maldonado, A. Ortiz, G. Paic and E. Perez, arXiv:1404.2372 [hep-ph].

[8] A. Ortiz, G. Paic and E. Cuautle, Nucl. Phys. A **941**, 78 (2015).

[9] A. Ortiz, arXiv:1705.02056 [hep-ex].

[10] T. Sjostrand, S. Mrenna and P. Z. Skands, JHEP **0605**, 026 (2006).

[11] Pythia8 online manual:(http://home.thep.lu.se/ torbjorn/pythia81html/Welcome.html).

[12] A. Ortiz Velasquez, P. Christiansen, E. Cuautle Flores, I. Maldonado Cervantes and G. Paic, Phys. Rev. Lett. **111**, 042001 (2013).

[13] P. Skands, S. Carrazza and J. Rojo, arXiv:1404.5630 [hep-ph].

[14] B. B. Abelev *et al.* [ALICE Collaboration], Int. J. Mod. Phys. A **29**, 1430044 (2014).

[15] S. Tripathy [ALICE Collaboration], arXiv:1807.11186 [hep-ex].

[16] C. Michael and L. Vanryckeghem, J. Phys. G **3** L151 (1977).

[17] R. Hagedorn, Riv. Nuovo Cim. **6N10**, 1 (1983).

[18] B. I. Abelev *et al.* (STAR Collaboration), Phys. Rev. C **75**, 064901 (2007).

[19] A. Adare *et al.* (PHENIX Collaboration), Phys. Rev. C **83**, 064903 (2011).

[20] K. Aamodt *et al.* (ALICE Collaboration), Eur. Phys. J. C **71**, 1655 (2011).

[21] B. Abelev *et al.* (ALICE Collaboration), Phys. Letts. B **717**, 162 (2012).

[22] B. Abelev *et al.* (ALICE Collaboration), Phys. Letts. B **712**, 309 (2012).

[23] S. Chatrchyan *et al.* (ALICE Collaboration), Eur. Phys. J. C **72**, 2164 (2012).

[24] E. Schnedermann, J. Sollfrank and U. W. Heinz, Phys. Rev. C **48**, 2462 (1993).

[25] P. Huovinen, P. F. Kolb, U. W. Heinz, P. V. Ruuskanen and S. A. Voloshin, Phys. Lett. B **503**, 58 (2001).

[26] P. Braun-Munzinger, J. Stachel, J. P. Wessels and N. Xu, Phys. Lett. B **344**, 43 (1995).

[27] Z. Tang *et al.*, Chin. Phys. Lett. **30** (2013) 031201.

[28] K. Adcox *et al.* [PHENIX Collaboration], Phys. Rev. C **69**, 024904 (2004)

[29] S. Acharya *et al.* [ALICE Collaboration], arXiv:1807.11321 [nucl-ex].

[30] G. Bencedi [ALICE Collaboration], arXiv:1807.09508 [hep-ex].

[31] J. Adam *et al.* [ALICE Collaboration], Eur. Phys. J. C **75**, 226 (2015).

[32] B. B. Abelev *et al.* [ALICE Collaboration], Phys. Lett. B **736**, 196 (2014).